ELSEVIER

J. Non-Newtonian Fluid Mech. 110 (2003) 177–193

Journal of Non-Newtonian Fluid Mechanics

www.elsevier.com/locate/jnnfm

Vortex shedding in cylinder flow of shear-thinning fluids II. Flow characteristics☆

P.M. Coelho, F.T. Pinho*

Faculdade de Engenharia da Universidade do Porto, DEMEGI, Rua Dr. Roberto Frias, 4200-465 Porto, Portugal

Received 29 July 2002; received in revised form 3 January 2003; accepted 8 January 2003

Abstract

A detailed experimental study on the flow characteristics of various vortex shedding regimes was carried out for the flow of non-Newtonian fluids around a cylinder. The fluids were aqueous solutions of carboxymethyl cellulose (CMC) and tylose at weight concentrations ranging from 0.1 to 0.6%, which had varying degrees of shear-thinning and elasticity. Two cylinders of 10 and 20 mm diameter were used in the experiments, defining an aspect ratio of 12 and 6 and producing blockages of 5 and 10%, respectively. The Reynolds number (*Re*) ranged from 50 to 9×10^3.

Shear-thinning gave rise to a decrease of the cylinder boundary-layer thickness and to a reduction of the diffusion length (l_d), which raised the Strouhal number, *St*. In the laminar shedding regime, a modified Strouhal number was successful at overlapping the shedding frequency variation with the Reynolds number for the various solutions. In contrast, fluid elasticity was found to increase the formation length (l_f), and this contributed to a decrease of the Strouhal number. The overall effect of shear-thinning and elasticity was an increase in the Strouhal number.

The increase in polymer concentration and the corresponding increase in fluid elasticity were responsible for the reduction of the critical Reynolds number marking the sudden decrease of the formation length, Re_{l_f}. In the shear layer transition regime, the formation length and Strouhal number data collapsed onto single curves as function of a Reynolds number difference, which confirmed Coelho and Pinho (J. Non-Newtonian Fluid Mech. (2003), accepted for publication) finding that an important effect of fluid rheology was in changing the demarcations of the various flow regimes.

Keywords: Shear-thinning; Non-Newtonian fluids; Cylinder flow; Laminar and transition vortex shedding

1. Introduction

There is widespread interest in investigating cylinder flows both due to their immediate industrial interest, in heat exchangers for instance, as well as to their fundamental nature. The literature is rich on

☆ The notation used throughout this paper is the same used in the first part of this work [1], to which the following new variables have been added.

* Corresponding author. Tel.: +351-225-081-762; fax: +351-225-081-763/445.
E-mail addresses: pmc@fe.up.pt (P.M. Coelho), fpinho@fe.up.pt (F.T. Pinho).

0377-0257/03/$ – see front matter © 2003 Elsevier Science B.V. All rights reserved.
doi:10.1016/S0377-0257(03)00008-9

Nomenclature

$Re^*_{l_f}$	Reynolds number corresponding to the strong decrease in l_f
l_{fc}	critical formation length: formation length just prior to its sudden drop (m)

Symbology in figures

×	water
+	glycerine and water mixture
●	0.4% CMC
▲	0.3% CMC
◆	0.2% CMC
■	0.1% CMC
○	0.6% tylose
△	0.4% tylose
◇	0.3% tylose
□	0.2% tylose

this subject, in particular when referring to Newtonian fluids, as can be assessed by various recent reviews [2,3].

For non-Newtonian fluids the literature is scarcer, especially regarding high Reynolds numbers flows. Shah et al. [4] were among the first to experimentally investigate cross flows of elastic aqueous solutions of carboxymethyl cellulose (CMC) up to Reynolds numbers of 12,000. Vortex shedding on cylinder flows of very dilute polymer solutions at a constant Reynolds number of 240 was also studied in the 1960s by Gadd [5]. Kalashnikov and Kudin [6] extended Gadd's work to a Reynolds number of 400 and investigated the effect of cylinder diameter. These were followed by the works of James and Acosta [7] and James and Gupta [8] which were limited to maximum Reynolds numbers of 50 and 200 and included heat transfer and drag measurements. More extensive reviews on previous Newtonian and non-Newtonian cylinder flow investigations at high Reynolds numbers have been presented by Coelho [9] and in the first part of this work [1].

This paper is a continuation of the experimental work of Coelho and Pinho [1], who identified and delimited the various vortex shedding regimes as a function of the Reynolds and elasticity numbers. Those flow regimes were the laminar, transition and shear layer transition regimes. In the present manuscript the flow characteristics within each of the identified flow regimes are analysed in detail.

In the next section the experimental facility and the main fluid characteristics are briefly described; more details are presented in [1]. At the beginning of Section 3 we summarise the flow regimes demarcated in [1] after which the new results are presented and discussed.

2. Experimental facility and fluid characteristics

The flow measurements were carried out in a water tunnel having a 6:1 contraction before a transparent test section of 197 mm height and 120 mm width. Two cylinders were used in the experiments: one had

Table 1
Main characteristics of the laser-Doppler anemometer

Laser wavelength (nm)	827
Laser power (mW)	100
Measured half angle of beams in air	3.68
Measuring volume size in water (e^{-2} intensity)	
Minor axis (μm)	37
Major axis (μm)	550
Fringe spacing (μm)	6.44
Frequency shift (MHz)	2.0

a diameter of 19.7 mm, leading to a blockage of 10% and an aspect ratio, L/D, of 6:1, whereas the other had a diameter of 10 mm corresponding to a blockage of 5% and an aspect ratio of 12:1.

A diode fibre-optic laser-Doppler system from INVENT, model DFLDA, was used for the velocity measurements, the full description of which can be found in Stieglmeier and Tropea [10]. The S30 optical probe was used with a 120 mm focusing lens and the LDA main characteristics are listed in Table 1. The output of the avalanche photodiode was processed by a 1990C TSI counter using the single measurements per burst mode and the frequency validation criterion was set to 1% comparison. The validated signals had at least 2^5 cycles.

High and low molecular weight polymers were dissolved in water to produce elastic and weakly elastic shear-thinning fluids, respectively, and the results compared to those of two Newtonian fluids of different viscosities.

The weakly elastic fluids were aqueous solutions of 0.2, 0.3, 0.4 and 0.6% by weight concentration of a methyl hydroxyethyl cellulose, brand name tylose, grade MH 10,000 K from Hoechst, with a molecular weight of 6000 kg/kmol. The more elastic fluids were aqueous solutions of carboxymethyl cellulose sodium salt (CMC), grade 7H4C from Hercules, with a molecular weight of 300,000 kg/kmol, at weight concentrations of 0.1, 0.2, 0.3 and 0.4%. To prevent bacteriological growth and degradation 0.02% (w/w) of a biocide, Kathon LXE 1.5% from Rohm & Haas, was added to all solutions of CMC. The Newtonian fluid was a mixture of 40% water and 60% glycerine (w/w), having a viscosity of 0.0073 Pa s at 25 °C, the temperature at which all tests were carried out. The viscosity and other rheological properties of the non-Newtonian fluids are presented in more detail in part I [1].

3. Results and discussion

Three flow regimes were clearly identified and delimited for each fluid [1]: they were the laminar vortex shedding regime, the transition regime, which includes the A- and B-mode types of shedding mechanism; and the shear layer transition regime, where the laminar-turbulent transition takes place in the shear layers. Tables 6 and 7 in [1] summarise those findings by listing the various critical Reynolds numbers.

It is now possible to examine in detail the hydrodynamic flow characteristics within each regime. The Reynolds number is defined as $Re^* = \rho D U_\infty / \eta_{ch}$, where D, U_∞, ρ and η_{ch} stand for the cylinder diameter, free-stream velocity, fluid density and the characteristic shear viscosity, respectively. For reasons explained in [1], η_{ch} is calculated from the rheogram at a characteristic shear rate $\dot{\gamma}_{ch}$ equal to $U_\infty/2D$.

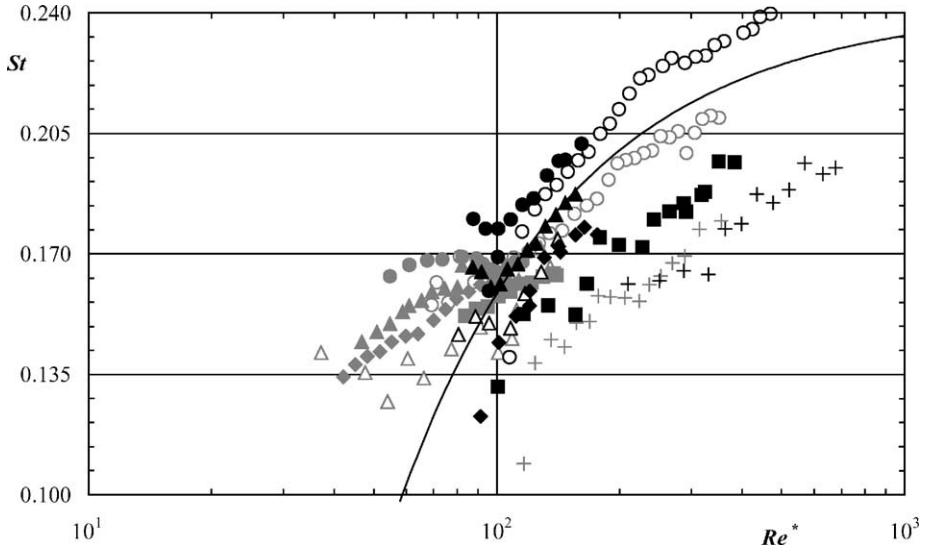

Fig. 1. Variation of the Strouhal number with Re^* and cylinder diameter in the laminar shedding regime (black symbols—20 mm cylinder; grey symbols—10 mm cylinder). Symbols as in symbology; full line: Henderson 2D calculations (Williamson [3]).

3.1. Laminar vortex shedding regime

Results of the normalised frequency shedding measurements (St), for both cylinders are compared in Fig. 1. The full line represents the Newtonian two-dimensional parallel ejection curve of Henderson [3] and the corresponding formation length results are shown in Fig. 2. The formation length (l_f) is the

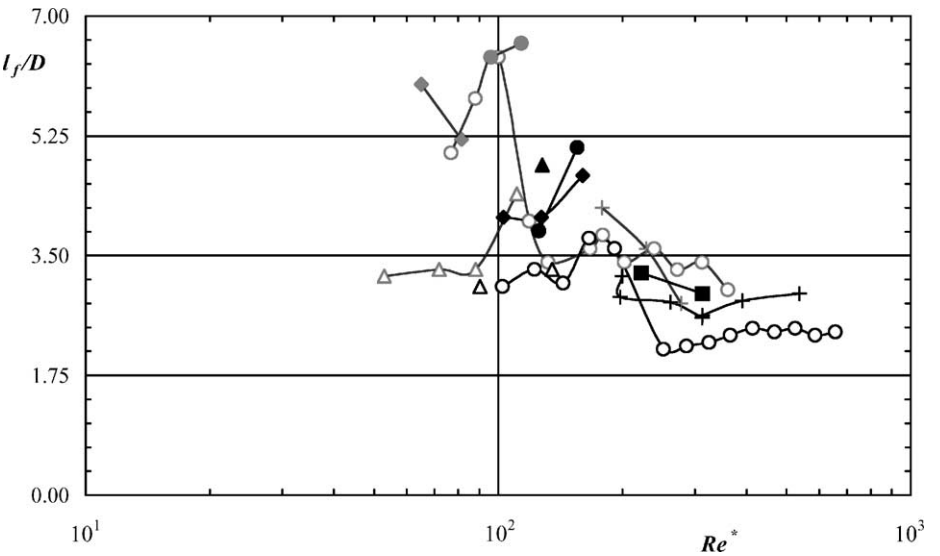

Fig. 2. Variation of the normalised formation length with Re^* and cylinder diameter in the laminar flow regime (black symbols—20 mm cylinder; grey symbols—10 mm cylinder). Symbols as in symbology.

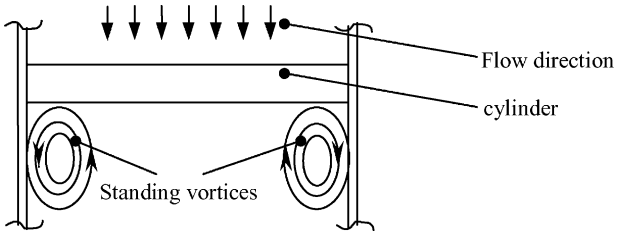

Fig. 3. Schematic representation of the fixed vortices observed in the flow of CMC solutions.

distance between the rear stagnation point and the locus of maximum velocity fluctuations. This location is difficult to measure at this flow regime, because of the broad peak of the $\overline{u'^2}$ profile along the wake, hence the higher experimental uncertainty in l_f here. For the 0.6% tylose solution the whole set of data was plotted because no signs of the transition regime were detected [1].

The variations of *St* for the CMC solutions are more sensitive to the cylinder diameter than those of the other Newtonian and non-Newtonian fluids but, in both cases, the Strouhal number increases with polymer concentration. There were no differences between the "increasing" and "decreasing" curves for the CMC solutions, whereas some histeresys was found for the 0.6% tylose and the viscous Newtonian flows with the 20 and 10 mm cylinder flows, respectively. Visual inspection of the flows showed the existence of fixed vortices at the edges of the cylinder for the flows of CMC only, as sketched in Fig. 3. So, the end effects are clearly different for the CMC flows and all other flows.

A possible cause for the increase in Strouhal number with polymer concentration would be a progressive reduction in the vortex shedding angle, but this was rejected as it would imply variations in excess of 30° (for instance, when comparing 0.4% CMC with the glycerine–water mixture) not seen in the flow visualisations. More relevant is the fact that some data are above the Henderson curve which pertains to Newtonian parallel shedding without end effects. Since end effects are also known to reduce frequency shedding [11–13], this curve represents maximum values of *St* and data above it can only be caused by others effects, such as rheological effects.

Kalashnikov and Kudin [6], Usui et al. [14] and more recently Cadot and Kumar [15] and Oliveira [16], reported reductions in Strouhal number with viscoelastic fluids having constant and weakly shear-thinning viscosity. On the other hand, according to Serth and Kiser [17] and Skelland [18] the boundary-layer thins with shear-thinning. Since Gerrard [19] and Berger and Wille [20] have shown the Strouhal number to be inversely proportional to the thickness of the shear layer, and hence to the thickness of the boundary-layer over the cylinder, the observed increase in Strouhal number with polymer concentration of Fig. 1 suggests that the effect of increased shear-thinning is stronger than the opposite effect of fluid elasticity.

Given these effects of shear-thinning on the normalised boundary-layer thickness (δ/s) and on the Strouhal number, an attempt was made to obtain less scattered representations of these non-dimensional quantities by combining them with a parameter quantifying the shear-thinning intensity, the power law index *n*. Simple linear and inverse linear dependencies were assumed between δ/s and *St* on one side and *n* on the other. The variations of δ/sn and $St\,n$ with the Reynolds number are plotted in Figs. 4 and 5, respectively and for a single cylinder in order to eliminate L/D effects.

The data in Fig. 4 show less scatter than the δ/s plot of Fig. 20 of Coelho and Pinho [1] and now the data of the tylose and CMC solutions are clearly distinct, suggesting that fluid properties other than

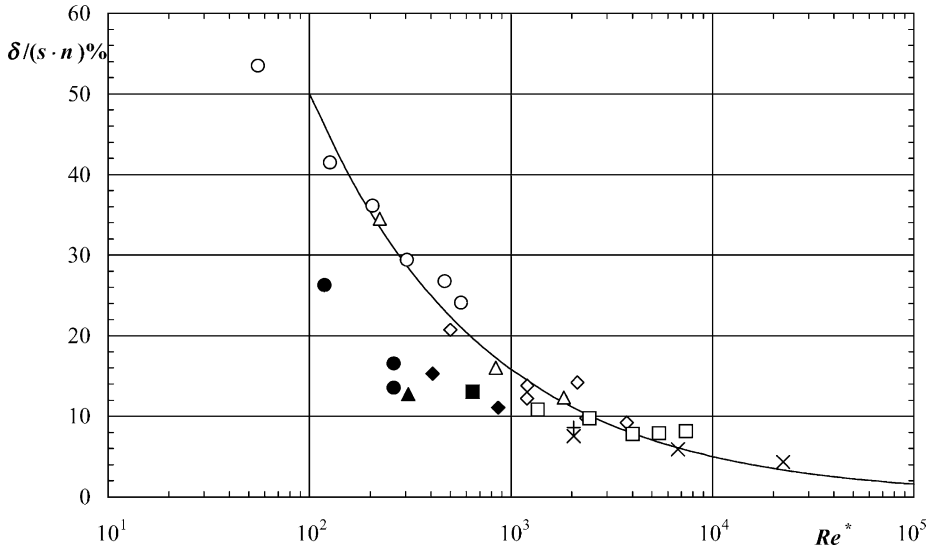

Fig. 4. Variation of the corrected thickness of the boundary-layer, δ/sn, at $\phi = 75^\circ$, with the Reynolds number for the 20 mm cylinder. Symbols as in symbology. Boundary-layer was assumed to end when $\partial u/\partial r = 0$.

shear-thinning are relevant. The full line corresponds to Blasius equation and was represented simply to help read and compare the figures.

In the new representation of the normalised shedding frequency in Fig. 5 the non-Newtonian data collapsed and now the major distinction between Newtonian and non-Newtonian data is fluid elasticity. It is important to understand that this modification should be regarded as purely quantitative. There is no

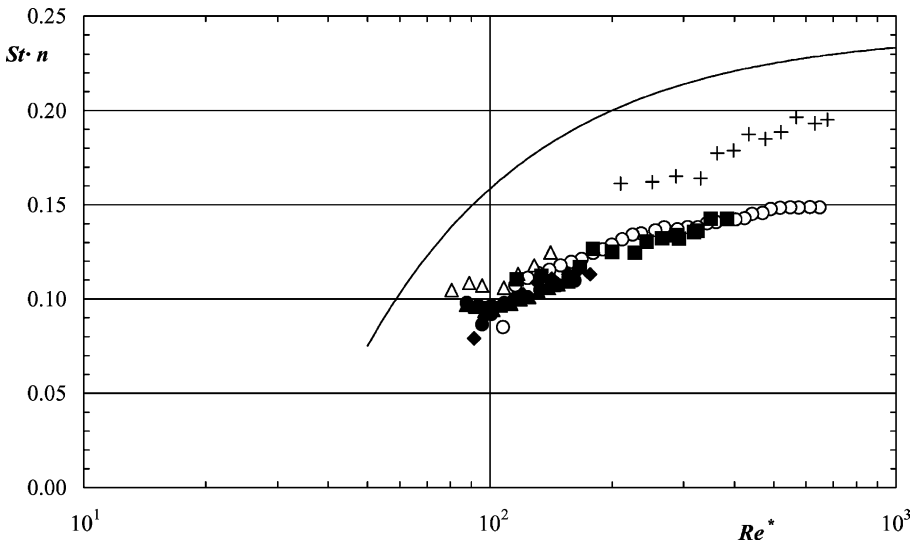

Fig. 5. Variation of the modified Strouhal number, $St\,n$, with Re^* in the laminar shedding regime for the 20 mm cylinder. Symbols as in symbology; full line: Henderson 2D calculations (Williamson [3]).

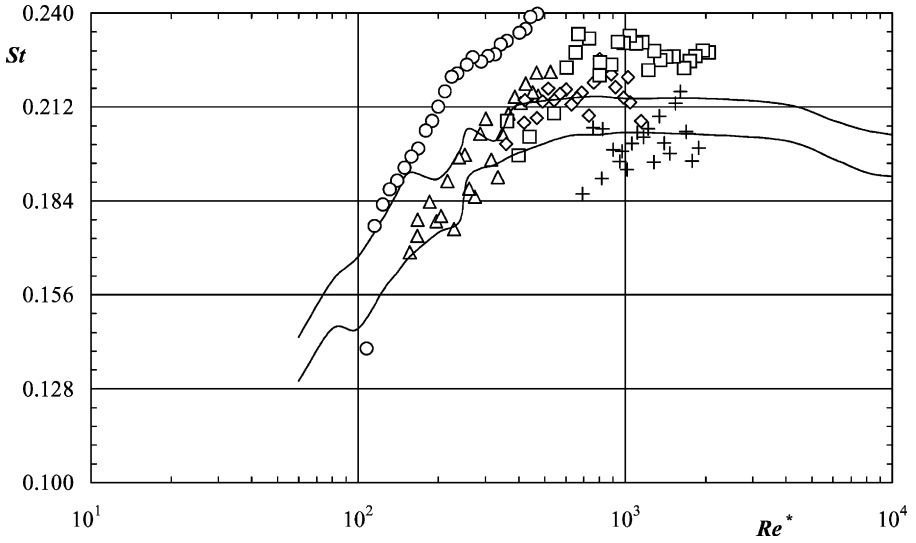

Fig. 6. Variation of the Strouhal number with Re^* in the transition regime for tylose solutions and 20 mm cylinder. Symbols as in symbology; full line: Unal and Rockwell [22].

reason to consider it as the correct way to account for shear-thinning instead of any other qualitatively similar modification (say, $\sqrt{n}\,St$).

The conflicting effects of shear-thinning and fluid elasticity have different origins. Whereas shear-thinning reduces the diffusion length, thus increasing the shedding frequency, fluid elasticity is responsible for an increase in the formation length, which tends to reduce the shedding frequency. Cadot and Kumar [15], Oliveira [16] and Cadot and Lebey [21] all observed an increase in the formation length with fluid elasticity, and here this was also found as will be shown later in Section 3.4.

3.2. Transition regime

The variation of the Strouhal number with the Reynolds number is plotted in Figs. 6 and 7 for the tylose and the CMC solutions, respectively. To help in the comparisons both figures include Newtonian data and the curves of Unal and Rockwell [22] and Fig. 7 also includes data for the 10 and 20 mm cylinders. The corresponding plots of the formation length are presented in Fig. 8 and $St\,n$ data are represented in Fig. 9 for the 20 mm cylinder.

For the 0.2 and 0.3% tylose solutions the onset of the transition regime could not be clearly defined [1] therefore, in these plots, values of Re^* equal to 355 and 139 were assumed for the 20 and 10 mm diameter cylinders, respectively. These values are those that were measured for the 0.1% CMC solution which, of all fluids measured, had the closest rheological behaviour to the two tylose solutions, i.e. low elasticity and shear-thinning intensity.

For the tylose solutions the Strouhal number variation in Fig. 6 has similarities to what was seen in the laminar shedding regime in that higher polymer concentration increases the shedding frequencies. The transitional nature of the flow is reflected in a higher degree of data scatter in comparison to what was seen in the laminar shedding regime. For the CMC solutions the picture is different because the data plotted in Fig. 7 tend to collapse at higher Reynolds numbers.

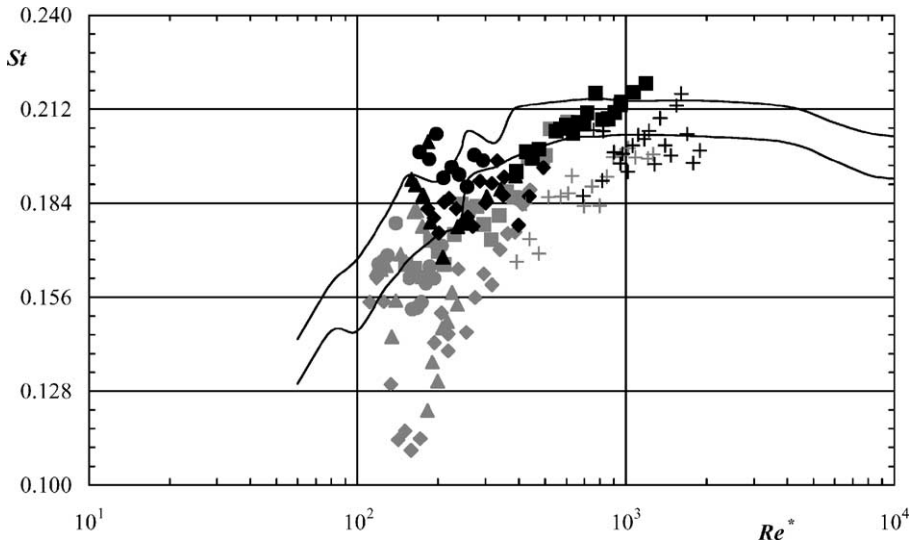

Fig. 7. Variation of the Strouhal number with Re^* and cylinder diameter in the transition regime for CMC solutions (black symbols—20 mm cylinder; grey symbols—10 mm cylinder). Symbols as in symbology; full line: Unal and Rockwell [22].

Fig. 8 shows a strong decrease in formation length for all the CMC solutions and the 0.6% tylose solution, which takes place well before the end of the transition regime. For this tylose solution Coelho and Pinho [1] observed that it was not possible to identify the transition regime. With the other tylose solutions and the Newtonian fluids, the strong decrease in l_f that marks the onset of the shear layer transition regime is observed at Reynolds numbers beyond the transition regime. This was already reported by [1],

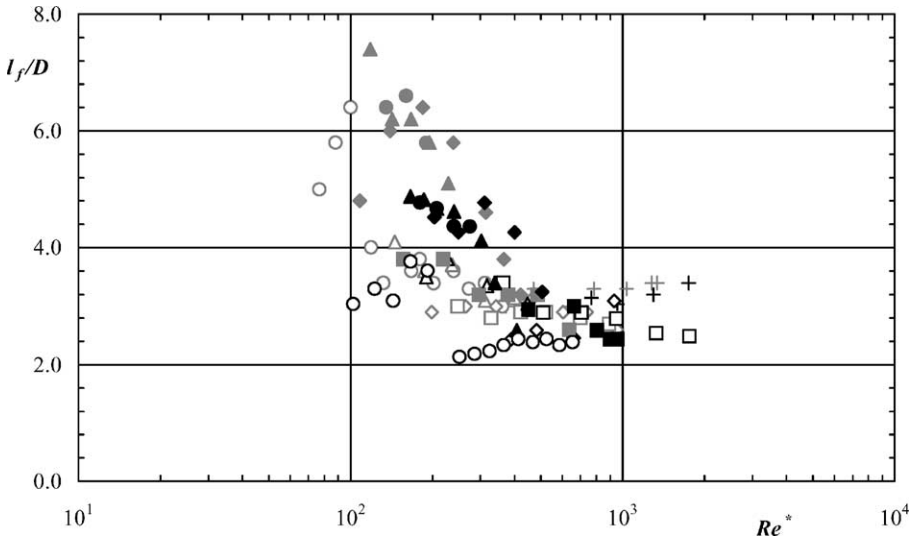

Fig. 8. Variation of the formation length with Re^* and cylinder diameter in the transition regime (black symbols—20 mm cylinder; grey symbols—10 mm cylinder). Symbols as in symbology.

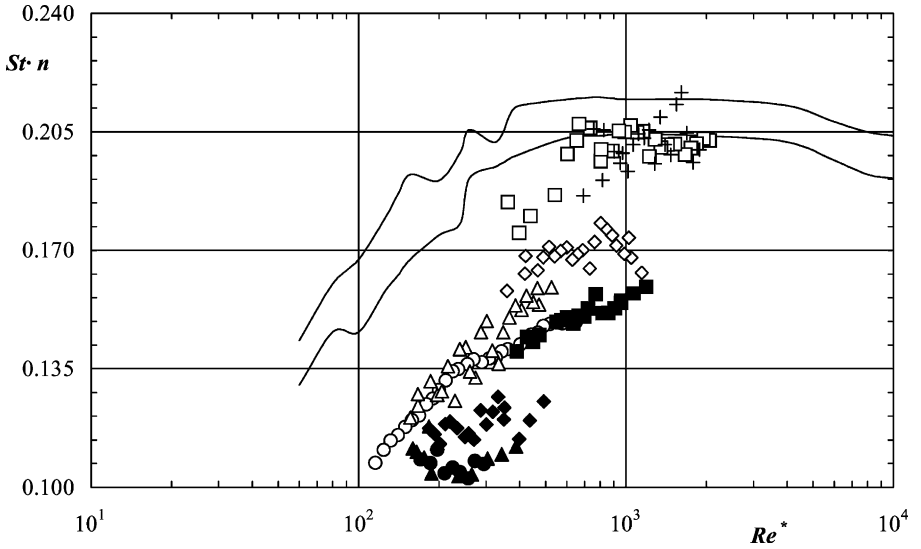

Fig. 9. Variation of the modified Strouhal number with Re^* in the transition regime for the 20 mm cylinder. Symbols as in symbology.

and it can also explain the other above-mentioned differences of flow behaviour between the tylose and CMC solutions. For all the tylose solutions, except the 0.6% fluid, l_f/D does not change appreciably and the shear layers remain laminar, therefore the diffusion length and the Strouhal numbers are affected by the polymer concentration as in the laminar vortex shedding regime. For the 0.6% tylose and all the CMC solutions, however, the sudden decrease in l_f/D has either just occurred or is imminent, i.e. in the transition regime the shear layers are being affected by instabilities, which, for the case of the CMC, are strengthened by the presence of the standing vortices sketched in Fig. 3. These instabilities tend to homogenise the behaviour of the CMC solutions.

The modified Strouhal number $St\,n$ is plotted in Fig. 9 for the 20 mm cylinder, showing that the collapse of data seen in the laminar regime no longer exists. This collapse has ceased because the diffusion length is now more affected by the downstream turbulence and the role of shear-thinning effects has diminished. This was also observed, but to a higher extent, at higher Reynolds numbers pertaining to the shear layer transition regime.

Except at 0.6% concentration, the formation length for all tylose solutions remains fairly constant and independent of the cylinder diameter. For the 0.6% tylose, however, the variations in l_f are akin to those experienced by the CMC solutions, i.e. now l_f increases with a decrease of the cylinder diameter.

The different behaviour of CMC and 0.6% tylose relative to the other tylose solutions is due to the dominant role of the instabilities in the shear layer which are less important with the latter flows. However, when the elasticity of the CMC solutions is reduced by lowering the polymer concentration to, say 0.1%, the flow behaviour of the CMC solutions tends to that of the less elastic tylose solutions. Note also that, external influences such as those of the standing vortices, are enhanced by a decrease in cylinder diameter. This increases the scatter of the Strouhal number data (Fig. 7) because the shear layers tend to interact more easily and the longer normalised formation lengths are also more sensitive to outside disturbances.

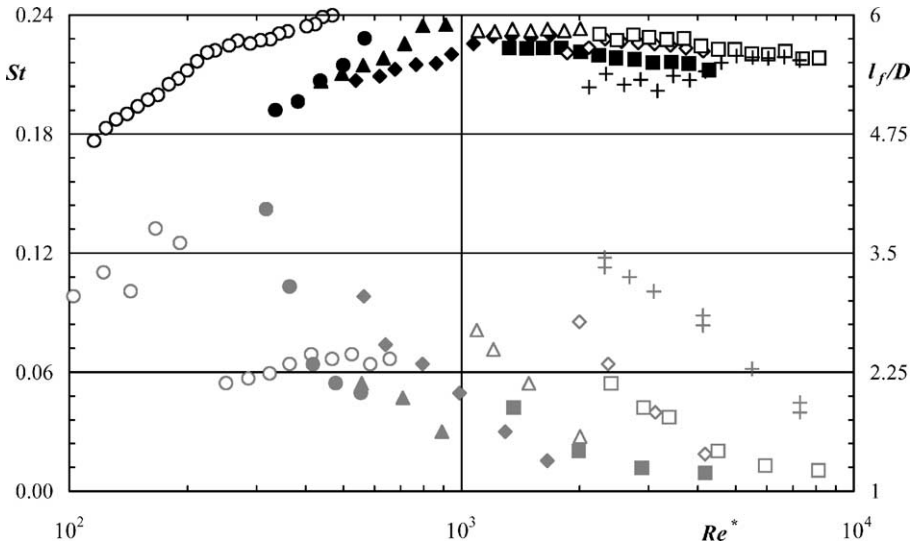

Fig. 10. Variation of the Strouhal number (black symbols) and normalised formation length (grey symbols) with Re^* for the 20 mm cylinder in the shear layer transition regime. Symbols as in symbology.

3.3. Shear layer transition regime

The variations of Strouhal number and formation length with Reynolds number are presented together in Figs. 10 and 11 for the 20 and 10 mm diameter cylinders, respectively. This is the flow regime where the shedding frequencies reach their maximum values.

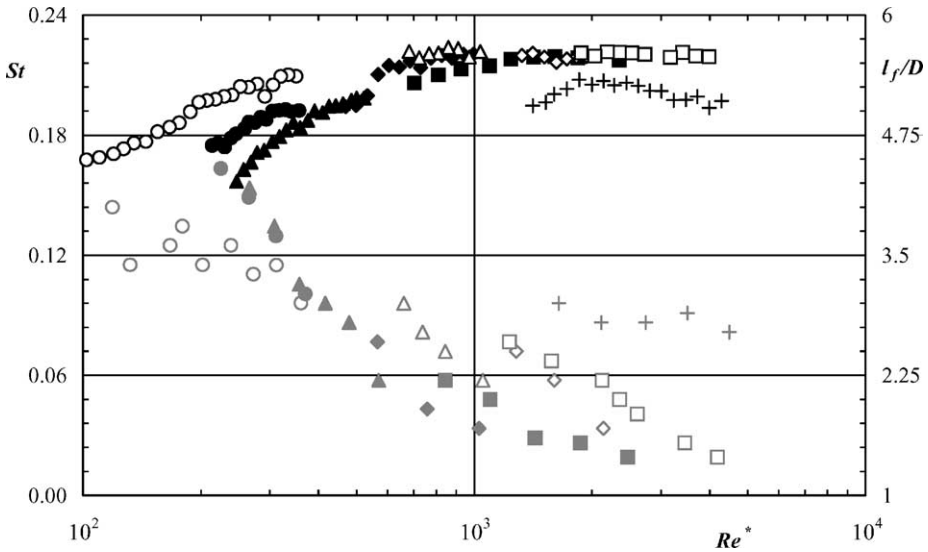

Fig. 11. Variation of the Strouhal number (black symbols) and normalised formation length (grey symbols) with Re^* for the 10 mm cylinder in the shear layer transition regime. Symbols as in symbology.

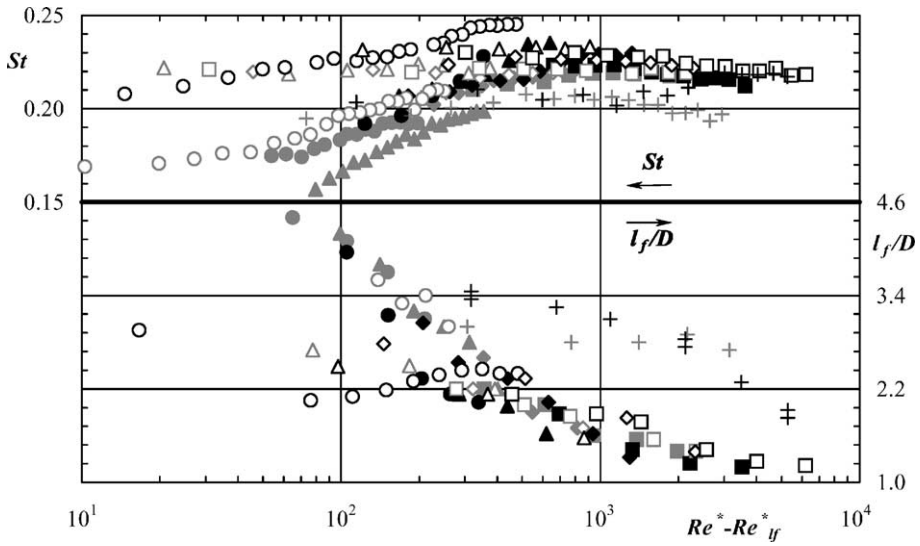

Fig. 12. Variation of the Strouhal number and normalised formation length with $(Re^* - Re^*_{l_f})$ for both cylinders (black symbols—20 mm cylinder; grey symbols—10 mm cylinder). Symbols as in symbology.

For each polymer both figures show a decrease in the formation length and an increase in Strouhal number with additive concentration, but less so with tylose. The data also shift to lower Reynolds numbers. However, when comparing solutions made from different polymers, a reduction in formation length is not synonymous of a larger Strouhal number, as shown in comparisons between the 0.2% CMC and 0.4% tylose solutions in Fig. 10 and between 0.1% CMC and 0.2% tylose in Fig. 11.

Coelho and Pinho [1] reported a strong decrease of l_f with Re^* for all solutions and related this variation to the transition in the shear layer, which, in turn, increases the diffusion length. Since this sudden drop does not occur at the same Reynolds number for all fluids, significant differences between diffusion lengths for the various flows at the same Reynolds numbers are expected. This must be taken into account in the above comparisons of results of solutions made of different polymers.

In order to eliminate the diffusion length effect, the Strouhal number and formation length are replotted in Fig. 12 as a function of the difference $(Re^* - Re^*_{l_f})$, where $Re^*_{l_f}$ is the Reynolds number corresponding to the critical formation length (l_{fc}/D). The critical formation length l_{fc} corresponds to the value of l_f just prior to its sudden drop. As shown in [1], for Newtonian and some non-Newtonian fluids the beginning of the shear layer transition is characterised by this strong decrease in formation length and although for some other elastic fluids that is not the case, strong influences upon the diffusion length are also expected when $Re^*_{l_f}$ is reached. By using this difference of Reynolds numbers, for identical values of $Re^* - Re^*_{l_f}$ there are good chances that the diffusion lengths of different fluid flows will be similar as they are at approximately the same developing stage relative to $Re^*_{l_f}$.

Clearly, for each fluid there is now a fairly good collapse of l_f/D and Strouhal number data regardless of cylinder diameter, except for 0.6% tylose and 0.3% CMC with the 10 mm cylinder. It may thus be concluded that within this flow regime there are no major differences between the flow characteristics of the tylose and the CMC solutions, except that the onset of the regime is strongly dependent on fluid rheology and cylinder diameter.

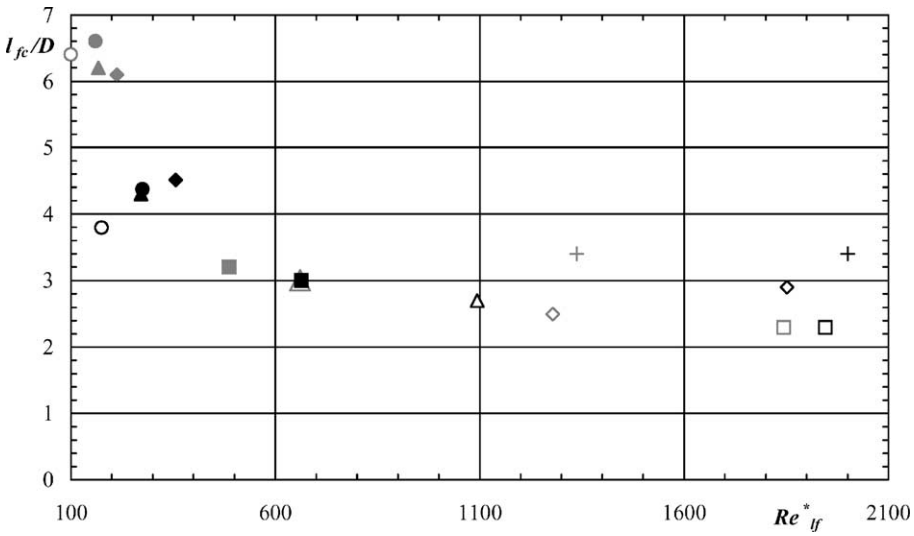

Fig. 13. Normalised formation length at onset of its sudden drop, l_{fc}/D, vs. Reynolds number (black symbols—20 mm cylinder; grey symbols—10 mm cylinder). Symbols as in symbology.

In Fig. 13 the value of the normalised critical formation length (l_{fc}/D) is plotted against the corresponding Reynolds number for all fluids. This figure shows an indirect proportionality between l_{fc}/D and $Re^*_{l_f}$, i.e. to the higher values of l_{fc}/D correspond earlier transitions in the shear layer. This is a consistent trend, because transition to turbulence moves upstream towards the cylinder from its wake as the Reynolds number increases, thus a larger formation length is accompanied by an earlier transition in the shear layer.

As shown by [1] with all CMC solutions, the critical formation length took place at lower Re^* pertaining to the transition regime. In these flows the shear layers were longer and more sensitive to Kelvin–Helmholtz instabilities that usually initiate shear layer transition. As a consequence, the shear layers of the CMC solutions in the transition regime were capable of entraining more fluid from the formation region and thus of starting the sudden reduction of l_f/D. At least for the CMC solutions, flow characteristics typical of both the transition and the shear layer transition regimes coexist for some time. Fig. 13 also shows that the values of l_{fc}/D increase with polymer concentration, especially for tylose, and with a reduction in cylinder diameter. Both effects are related to fluid elasticity as will be seen in the next section.

Curves were fitted to the l_f/D versus $Re^* - Re^*_{l_f}$ data pertaining to the tylose and CMC solutions shown in Fig. 12, but in log–log coordinates and excluding the 0.6% tylose data. The slope of the fittings to the CMC data was higher suggesting that the upstream propagation of the shear layer transition with Reynolds number is faster with the CMC than with the tylose solutions ($\text{CMC}_{\text{slope}} = -0.371$, $\text{tylose}_{\text{slope}} = -0.201$).

In Fig. 14 the dimensionless parameter l_f/l_{fc} is plotted as a function of $Re^* - Re^*_{l_f}$. The more elastic solutions of CMC and 0.6% tylose show the highest relative reduction in the formation length, whereas the smallest variations are those of the Newtonian fluid. These observations are consistent with and extend the findings of Cadot and Kumar [15] that fluid elasticity stabilise the shear layers. In fact, as the shear layers become turbulent it is expected that those that are more stable will suffer more intense modifications.

If the advance of the shear layer transition is very intense the transition regime can even be suppressed, as with the 0.6% tylose solution. This is not entirely surprising because, recently, Cadot and Kumar

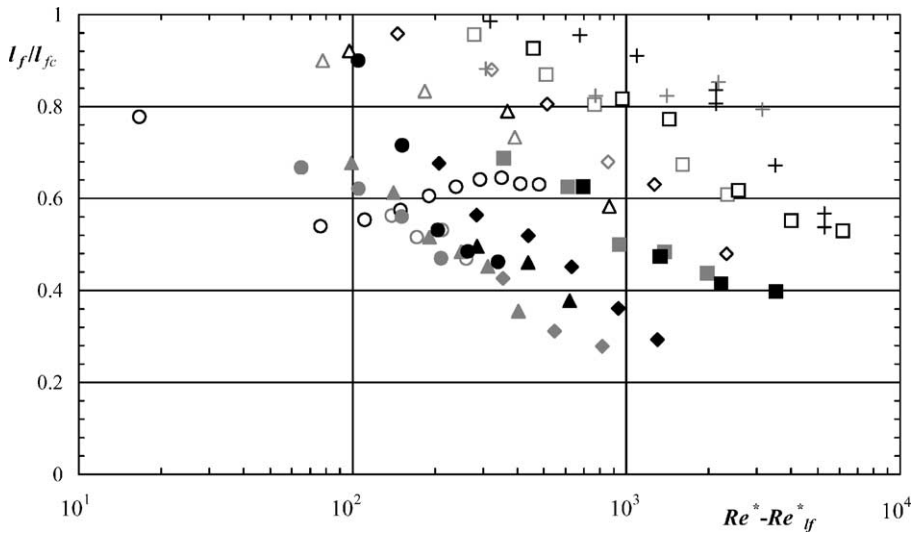

Fig. 14. Ratio of formation length l_f/l_{fc} as a function of Reynolds number (black symbols—20 mm cylinder; grey symbols—10 mm cylinder). Symbols as in symbology.

[15] observed the suppression of A-mode vortex shedding in the transition regime. In combination with an earlier shear layer transition, the suppression of the A-mode can altogether be responsible for the elimination of the intermediate transition regime. In fact, with this solution, the ratio of elastic to inertia forces is the highest in locations where the shear rates are high, as in the boundary-layer and the free shear layer, as shown by Coelho and Pinho [1].

For the 0.6% tylose solution, the Strouhal number and the formation length data of Fig. 12 follow the curves of the remaining fluids, especially for the 10 mm diameter cylinder. This suggests that there is also laminar-turbulent transition in the shear layers, although for this fluid the intermediate transition regime was not observed.

3.4. Relation between l_{fc}/D, $Re^*_{l_f}$ and elastic dimensionless numbers

In this section we investigate the effect of elasticity on the variations of the critical formation length (l_{fc}) and the corresponding Reynolds number. As mentioned above, this is the criterion marking the onset of shear layer transition for Newtonian fluids and was adopted by [1] for non-Newtonian fluids, as long as l_{fc} was observed under conditions not corresponding to those of the transition regime. To quantify fluid elasticity the Weissenberg number is used and is defined as $We \equiv \lambda_e U_\infty / D$, where λ_e represents the relaxation time of the fluid, U_∞ is the free-stream velocity and D is the cylinder diameter.

The variation of l_{fc}/D with We is represented in Fig. 15 where a good correlation is seen for the whole group of tylose solutions and independently of cylinder diameter. The corresponding fitted curve is also shown in the figure. For the CMC solutions, however the behaviour is quite different: there is now a diameter effect and, for each cylinder size, the shape of the curve differs from that for tylose. This diameter effect is caused again by the corresponding standing vortices located at the ends of the cylinder, on their downstream sides (see Fig. 3).

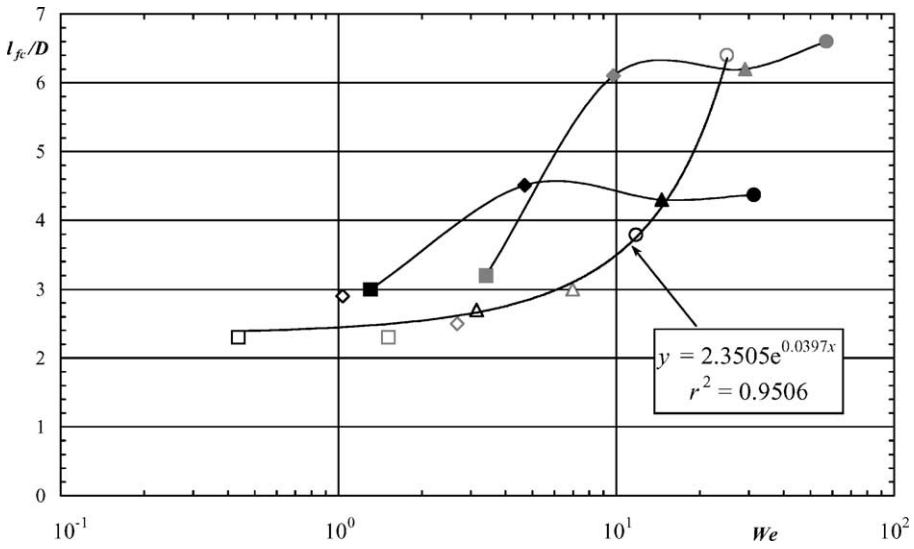

Fig. 15. Normalised formation length at onset of its sudden drop, l_{fc}/D, as a function of the Weissenberg number, *We* (black symbols—20 mm cylinder; grey symbols—10 mm cylinder). Symbols as in symbology.

Although the variations of l_{fc}/D with *We* are different for the two polymers, in both cases there is an increase in formation length with elasticity in agreement with Cadot and Lebey [21]. With CMC there is an increase in l_{fc}/D at low values of *We* followed by saturation. As also seen in Section 3.2, the standing vortices at the ends of the cylinder seem to cause flow instabilities in the shear layer and these also tend to level the frequency shedding, leading to constant values of Strouhal number and l_f/D. In contrast, no

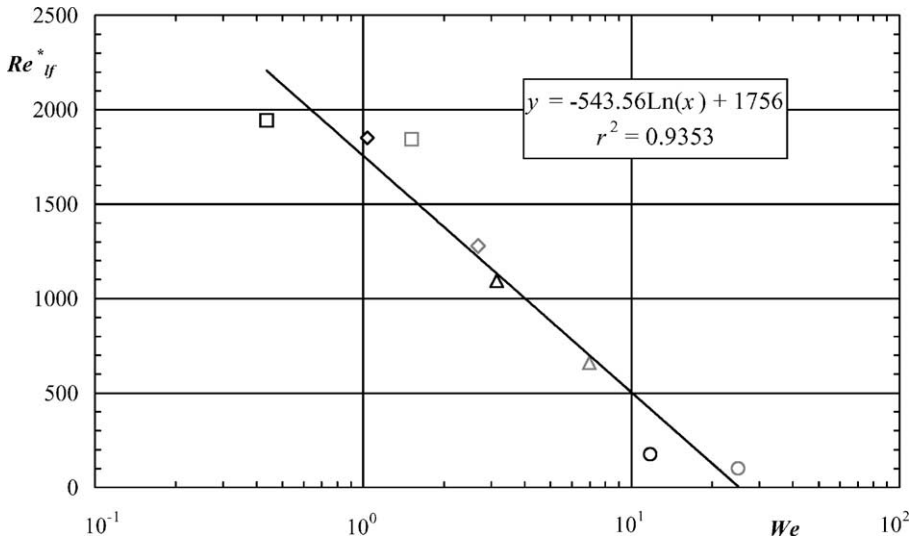

Fig. 16. Variation of Reynolds number at l_{fc}/D with the Weissenberg number for tylose solutions (black symbols—20 mm cylinder; grey symbols—10 mm cylinder). Symbols as in symbology.

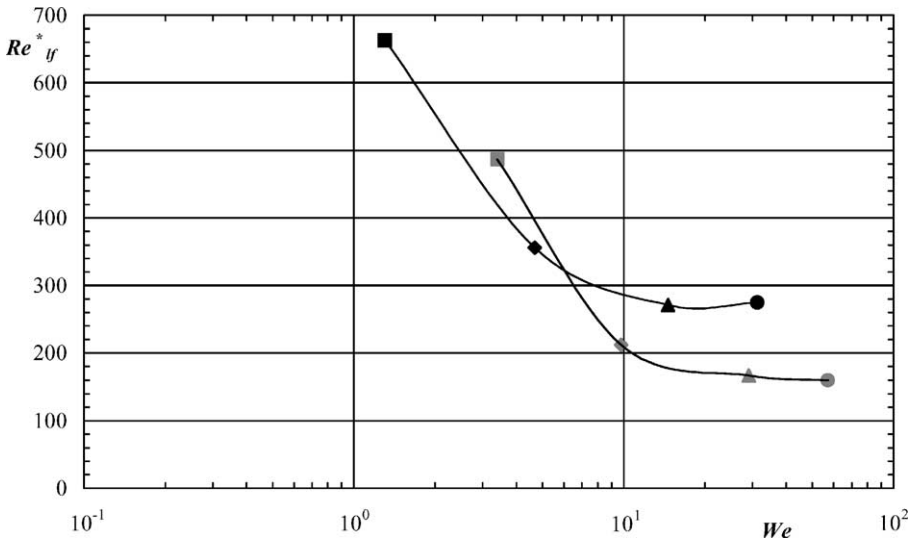

Fig. 17. Variation of Reynolds number at l_{fc}/D with the Weissenberg number for CMC (black symbols—20 mm cylinder; grey symbols—10 mm cylinder). Symbols as in symbology.

standing vortices were found for the tylose solutions where the saturation effect at high Weissenberg numbers is absent.

In Figs. 16 and 17 the variation of $Re^*_{l_f}$ with *We* is represented for tylose and CMC solutions, respectively. For the tylose solutions there is again a good correlation between both quantities, which is independent of cylinder diameter and is linear in semi-log coordinates. For the CMC solutions, in contrast, two distinct curves are observed, one for each cylinder. In both CMC cases, $Re^*_{l_f}$ initially decreases with elasticity and then levels off. Basically, the effects of *We* and cylinder diameter upon $Re^*_{l_f}$ are the inverse of those seen previously with l_{fc}/D and confirm that fluid elasticity advances shear layer transition and increases the formation length, but in different ways that depend on the polymer type.

4. Conclusions

Measurements of flow characteristics of aqueous solutions of tylose and CMC downstream of cylinders were obtained pertaining to the laminar, transition and shear layer transition regimes. The main findings were:

(i) In the laminar shedding regime shear-thinning reduces the boundary-layer thickness and the diffusion length, the latter increasing the Strouhal number. By modifying the Strouhal number as $St\,n$ it was possible to obtain a single curve of $St\,n$ versus Re^*.

(ii) Fluid elasticity was found to have the opposite effect to shear-thinning, reducing the vortex shedding frequency because it increased the formation length. In particular, for the fluids tested here, the effect of shear-thinning exceeded that of elasticity and the overall result was an increase in *St* with polymer concentration.

(iii) For the CMC solutions, flow visualisations showed the existence of standing vortices at the ends of the cylinder, on their downstream side. Such vortices were absent in the flows of tylose solutions. The different end conditions were responsible for the different hydrodynamic behaviour of tylose and CMC solutions, especially regarding cylinder diameter effects.

(iv) Fluid elasticity was found to increase the length of the formation region and for the 0.6% tylose solution it suppressed the transition regime. The larger formation regions are more sensitive to turbulence which, coupled with the suppression of the A-mode sub-regime [15], contribute to the advance of the end of the transition flow regime and even to its suppression.

(v) The normalised critical formation length (l_{fc}/D) was equal to 3.4 for Newtonian fluids, but increased with the Weissenberg number and was double for the more elastic fluids. Elasticity was found to increase the formation length due to its action on the shear layers: as observed by Cadot and Lebey [21], elasticity reduces the entrainment of fluid by the shear layers from the formation region.

(vi) The variations of l_{fc}/D and of the corresponding Reynolds number ($Re^*_{l_f}$) with fluid elasticity are closely linked. In particular, l_{fc}/D increases and $Re^*_{l_f}$ decreases with elasticity. Since transition to turbulence progresses from the wake towards the cylinder it is expected that a longer formation region will be subjected to flow instabilities at an earlier stage and this advances shear layer transition. As the polymer concentration and the fluid elasticity increase, the reduction of the formation length with the Reynolds number, relative to its initial value l_{fc}, is enhanced.

Acknowledgements

The authors wish to thank JNICT for the financial support through project PBIC/C/CEG/1370/92 and the equipment lent by INEGI and IDMEC. P.M. Coelho also wishes to thank University of Porto for the leave of teaching duties between 1993 and 1996 which made possible a significant portion of this work.

References

[1] P.M. Coelho, F.T. Pinho, Vortex shedding regimes in cylinder flow of shear-thinning fluids. I. Identification and demarcation, J. Non-Newtonian Fluid Mech. 110 (2–3) (2003) 149–182.
[2] D.P. Telionis, M. Gundappa, T.E. Diller, On the organisation of flow and heat transfer in the near wake of a circular cylinder in steady and pulsed flow, ASME J. Fluid Eng. 114 (1992) 348–355.
[3] C.H.K. Williamson, Vortex dynamics in the cylinder wake, Ann. Rev. Fluid Mech. 28 (1996) 477–539.
[4] M.J. Shah, E.E. Petersen, A. Acrivos, Heat transfer from a cylinder to a power-law non-Newtonian fluid, AIChE J. 8 (1962) 542–549.
[5] G.E. Gadd, Effects of long-chain molecule additives in water on vortex streets, Nature 211 (1966) 169–170.
[6] V.N. Kalashnikov, A.M. Kudin, Kármán vortices in the flow of drag-reducing polymer solutions, Nature 225 (1970) 445–446.
[7] D.F. James, A.J. Acosta, The laminar flow of dilute polymer solutions around circular cylinders, J. Fluid Mech. 42 (1970) 269–288.
[8] D.F. James, O.P. Gupta, Drag on circular cylinders in dilute polymer solutions, Chem. Eng. Prog. Symp. Ser. 67 (111) (1971) 62–73.
[9] P.M. Coelho, Flow of non-Newtonian fluids around a cylinder (in Portuguese), Ph.D. Thesis, University of Porto, Portugal, 2000.
[10] M. Stieglmeier, C. Tropea, A miniaturised, mobile laser-Doppler anemometer, Appl. Opt. 111 (1992) 4096–4099.
[11] M. Brede, H. Eckelmann, D. Rockwell, On secondary vortices in the cylinder wake, Phys. Fluids 8 (1996) 2117–2124.
[12] C.H.K. Williamson, Defining a universal and continuous Strouhal–Reynolds number relationship for the laminar vortex shedding of a circular cylinder, Phys. Fluids 31 (1988) 2742–2744.

[13] D. Gerich, H. Eckelmann, Influence of end plates and free ends on the shedding frequency of circular cylinders, J. Fluid Mech. 122 (1982) 109–121.
[14] H. Usui, T. Shibata, Y. Sano, Kármán vortex behind a circular cylinder in dilute polymer solutions, J. Chem. Eng. Jpn. 13 (1980) 77–79.
[15] O. Cadot, S. Kumar, Experimental characterisation of viscoelastic effects on two- and three-dimensional shear instabilities, J. Fluid Mech. 416 (2000) 151–172.
[16] P.J. Oliveira, Method for time-dependent simulations of viscoelastic flows: vortex shedding behind cylinder, J. Non-Newtonian Fluid Mech. 101 (2001) 113–137.
[17] R.W. Serth, K.M. Kiser, A solution of the two-dimensional boundary-layer equations for an Ostwald-de Waele fluid, Chem. Eng. Sci. 22 (1967) 945–956.
[18] A.H.P. Skelland, Non-Newtonian flow and heat transfer, Wiley, New York, 1967.
[19] J.H. Gerrard, The mechanics of the formation region of vortices behind bluff bodies, J. Fluid Mech. 25 (1966) 401–413.
[20] E. Berger, R. Wille, Periodic flow phenomena, Annu. Rev. Fluid Mech. 4 (1972) 313–340.
[21] O. Cadot, M. Lebey, Shear instability inhibition in a cylinder wake by local injection of a viscoelastic fluid, Phys. Fluids 11 (1999) 494–496.
[22] M.F. Unal, D. Rockwell, On vortex formation from a cylinder. Part 1. The initial instability, J. Fluid Mech. 190 (1988) 491–512.